Supporting information

Supporting Information

Inducing the Weak and Negative Jahn-Teller Distortions to Alleviate the Structural Deformation for Stable Sodium Storage

Zishan Hou,[a] Yuanming Liu,[a] Shuyun Yao,[a] Shiyu Wang,[a] Yingjie Ji,[a] Weijie Fu,[a] Jiangzhou Xie,[b] Yi-Ming Yan[a] and Zhiyu Yang*[a]

[a] State Key Laboratory of Organic-Inorganic Composites, Beijing Advanced Innovation Center for Soft Matter Science and Engineering, Beijing University of Chemical Technology, Beijing, 100029, People's Republic of China

[b] School of Mechanical and Manufacturing Engineering, University of New South Wales, Sydney, New South Wales 2052, Australia

*Corresponding authors.

E-mail address: yangzhiyu@mail.buct.edu.cn

Supporting information

Experimental Procedures

Chemicals and Materials

Potassium carbonate (K_2CO_3, 99%), Manganese (III) oxide (Mn_2O_3, 99%) were obtained from Shanghai Macklin Biochemical Co., Ltd. Magnesium oxide (MgO, 99%) were obtained from Aladdin Industrial Corporation. Anhydrous (Na_2SO_4) were purchased from Beijing Tong Guang Fine Chemicals Company. All reagents were used as received without further purification. And all solutions were prepared using ultrapure water (resistance = 18.2 MΩ cm).

Fabrication of Electrode Materials

In this work, $K_{0.5}MnO_2$ and $K_{0.5}Mn_{0.85}Mg_{0.15}O_2$, are denoted as KMO and KMMO, respectively. These materials were synthesized using a conventional high temperature solid-state reaction approach, employing stoichiometric precursors of K_2CO_3, Mn_2O_3 (99% purity), and MgO (99% purity). The precursors were meticulously ground in an agate mortar with 5 wt.% excess K_2CO_3. Subsequently, the powders were subjected to a heating process at 900 ℃ for 24 hours under an air atmosphere, with a heating rate of 2 ℃ min^{-1}. Following natural cooling to room temperature, the resulting samples were obtained.

Characterizations

The chemical compositions of the samples were determined by ICP analysis (ICP-OES, Agilent 725-ES). Microstructures were studied using scanning electron microscopy (SEM, FEI Quanta 200) at 20 kV, transmission electron microscopy (TEM; FEI Tecnai G2 20) and HRTEM (JEOL, JEM-2100, 200 kV). Magnetic force microscopy (MFM) technique (Japan Hitachi-AFM5100W) was used to visualize the magnetic properties of synthesized samples using a standard MFM tip coated with CoCr film (Japan Hitachi-AFM5100W), which was pre-magnetized. Magnetic property of samples was measured at room temperature with Physical Property Measurement System (PPMS-9: Quantum Design, SanDiego, CA, USA). JEOLJESFA200 EPR spectrometer was used to obtain the electron paramagnetic resonance (EPR) spectra, and operating parameters were 140K, 9064 MHz, 0.998 mW, X-band. The temperature magnetic susceptibility (M-T) curves were obtained using a MPMS3 Quantum Design SQUID physical property measurement system in the temperature region of 2 to 300 K. The in-situ XRD was tested using a Rigaku MiniFlex powder diffractometer (Cu Kα, λ = 0.154056 nm) at a scan rate of 0.02°/step and a scan range of 5 to 30°. Raman spectroscopy was performed on a 532 nm Finder Vista Laser micro-Raman Spectroscopy (Zolix, China). The electronic structure and compositional information on the samples were investigated by X-ray photoelectron spectroscopy (XPS, ESCALAB 250). The soft-XAS measurements were carried out in total electron yield mode under ultra-high vacuum at beamline 4B9B of Beijing Synchrotron Radiation Facility of the Institute of High Energy Physics, Chinese Academy of Sciences. Au 4f7/2 core level spectra were recorded for the photon energy calibration, and the energy resolution is better than 0.2 eV at room temperature. The electrochemical operando Cell (EC-RAIR-H) is supplied by Beijing Science Star technology Co. Ltd. The Raman spectrum was recorded on a HORIBA Raman microscope with a laser wavelength of 532 nm (LabRAM Aramis, HORIBA Jobin Yvon S.A.S, France) for surface characterization. Raman spectra of the sample (one spectrum per 30 s) were captured while a cyclic voltammetry test at a scan rate of 10 mV s^{-1} simultaneously.

Electrochemical Measurements

Working electrode was prepared by traditional slurry-coating method. 80 wt% active material, 10 wt% acetylene black and 10 wt% polytetrafluoroethylene (PTFE) was mixed and coated onto carbon cloth with an area of 1 cm^2. The electrode was then heated at 60 ℃ for 2 hours to evaporate the solvent and used as working electrode. The negative electrode was prepared by mixing active carbon, acetylene black and PTFE with a mass ratio of 8 : 1 : 1. Electrochemical measurements were conducted in a general three-electrode configuration in 1.0 M Na_2SO_4 aqueous electrolyte with Ag/AgCl and a Pt foil as reference electrode and counter electrode, respectively. Cyclic voltammetry (CV) and galvanostatic charge discharge (GCD) experiments were performed to determine the electrochemical properties of the electrodes in a potential window of -0.2 to 1.2 V. All the operating current densities were calculated based on the mass of the active materials Electrochemical

impedance spectroscopy (EIS) measurements were carried out by applying an AC voltage with 5 mV amplitude in a frequency range from 0.01 Hz to 100 kHz at open potential.

The specific capacitance C (F g^{-1}) was calculated based on the GCD curves according to equation[1]:

$$C = \frac{I \times \Delta t}{m \times V} \quad \text{(S1)}$$

where I (A) and Δt (s) are the discharge current and time, respectively, m (g) represents of the active material's loading mass and V refers to the charge/discharge potential window.

Sodium Diffusion Coefficient Calculation

The diffusion coefficient of Na^+(D_{Na+}) can be obtained from the low frequency line according to the equation[2]:

$$D_{Na+} = 0.5(RT/AF^2C\sigma)^2 \quad \text{(S2)}$$

where R, T, F, A, and C are the gas constant, the absolute temperature, the Faraday's constant, the apparent area of the electrode, and the molar concentration of Na^+, respectively. σ is the Warburg factor following equation:

$$Z' = Re + Rct + \sigma\omega^{-\frac{1}{2}} \quad \text{(S3)}$$

where Re is the resistance between the electrolyte and electrode, and Rct is the charge transfer resistance. Thus, the slopes of the plot of Z'vs $\omega^{-1/2}$ can used to obtain the values of σ.

Kinetic Calculation

Capacitance contribution can be qualitatively analyzed according to CV curve, as shown below:

$$i = av^b \quad \text{(S4)}$$

where i and v are the current density and the potential scan rate, respectively, α is a constant and b is a tunable parameter with a value of 0.5-1.0. When the value of b is close to 1.0, the reaction process is dominated by surface capacitance; when the value of b is close to 0.5, the reaction process is dominated by diffusion control.

The contribution of capacitance and diffusion limit to the total capacitance is further quantified.

$$i(V) = k_1v + k_2v^{1/2} \quad \text{(S5)}$$

where k_1 and k_2 represent capacitive and diffusion contributions, respectively.

Supercapacitor Devices Measurements.

Supercapacitor Devices Measurements: Asymmetric supercapacitor (ASC) device was fabricated by employing AC and com-MnO_2 as anode and cathode, respectively. Two electrodes were separated by glassy fibrous separator in 1 M Na_2SO_4 aqueous electrolyte. Cyclic voltammetry (CV) and galvanostatic charge/discharge (GCD) measurements were performed in a potential window of 0 to 2.0 V.

The energy density (*E*, Wh kg^{-1}) of the ASC is calculated according to S6[3]:

$$E = 0.125 \times C \times V^2 \quad \text{(S6)}$$

The power density (*P*, W kg^{-1}) of the ASC is calculated according to S7:

$$P = \frac{E \times 3600}{t} \quad \text{(S7)}$$

where *t* (s) is discharge time.

Computational Details.

All density functional theory (DFT) calculations within spin-polarized frame were performed using the Vienna Ab initio Simulation Package (VASP).[4, 5] The elemental core and valence electrons were represented by the projector augmented wave (PAW) method and plane-wave basis functions with a cutoff energy of 400 eV. Generalized gradient approximation with the Perdew-Burke-Ernzerhof (GGA-PBE) exchange-correlation functional was employed in all the calculations.[6] The DFT-D3 empirical correction method was employed to describe van der Waals interactions. Geometry optimizations were performed with the force convergency smaller than 0.07 eV/Å. Monkhorst-Pack k-points of 1×1×1 was applied for all the

calculations.

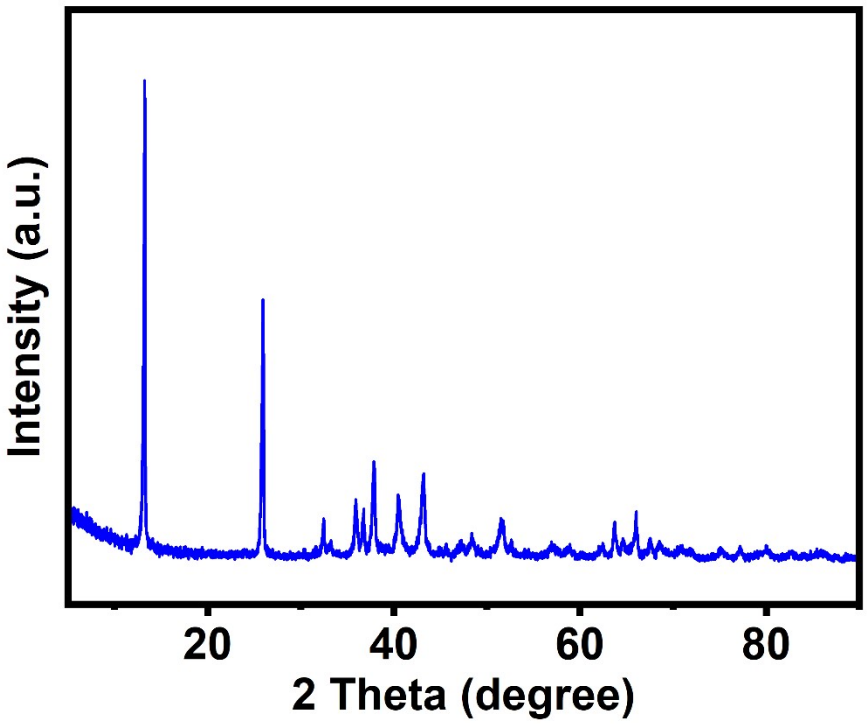

Figure S1. XRD pattern of KMO.

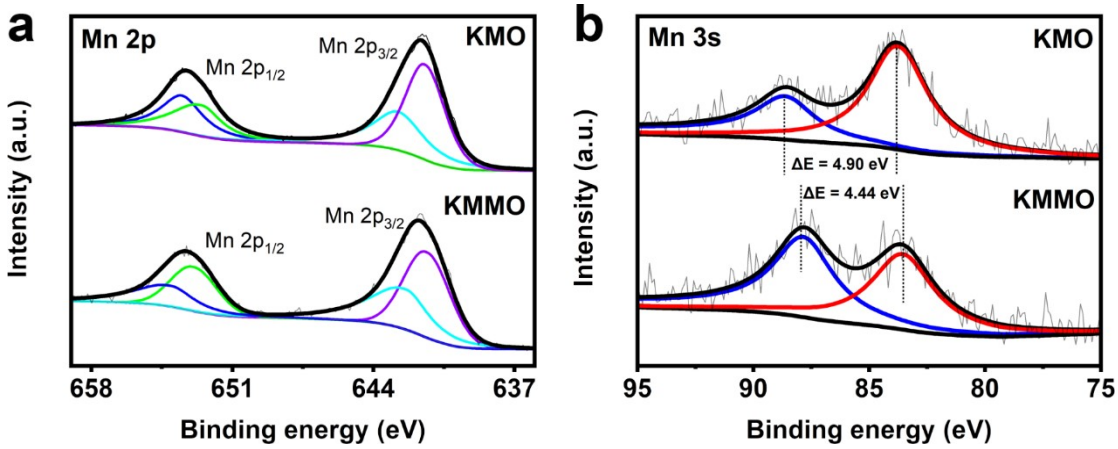

Figure S2. XPS spectra of a) Mn 2p and b) Mn 3s.

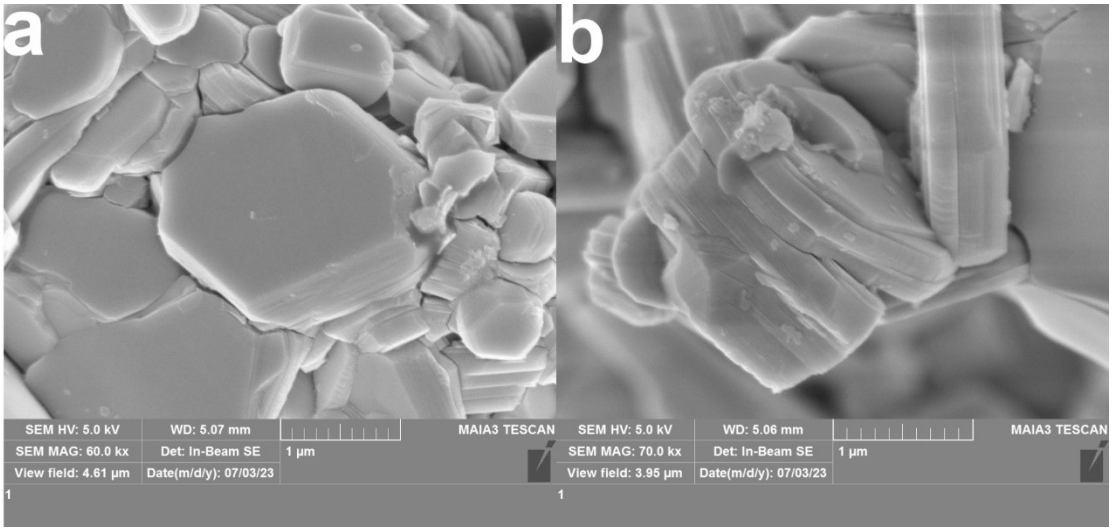

Figure S3. SEM images of KMO.

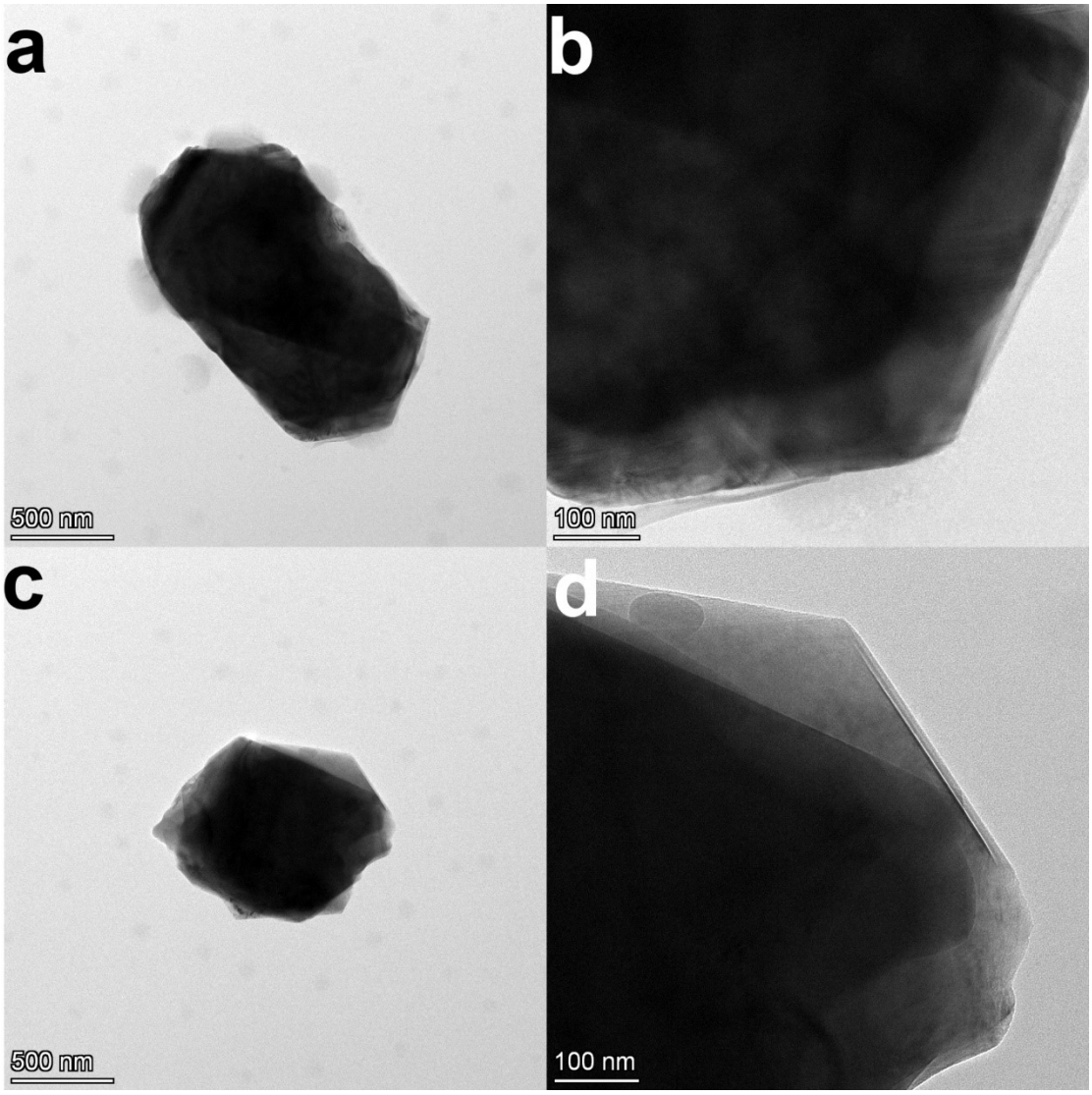

Figure S4. TEM images of a, b) KMO and c, d) KMMO.

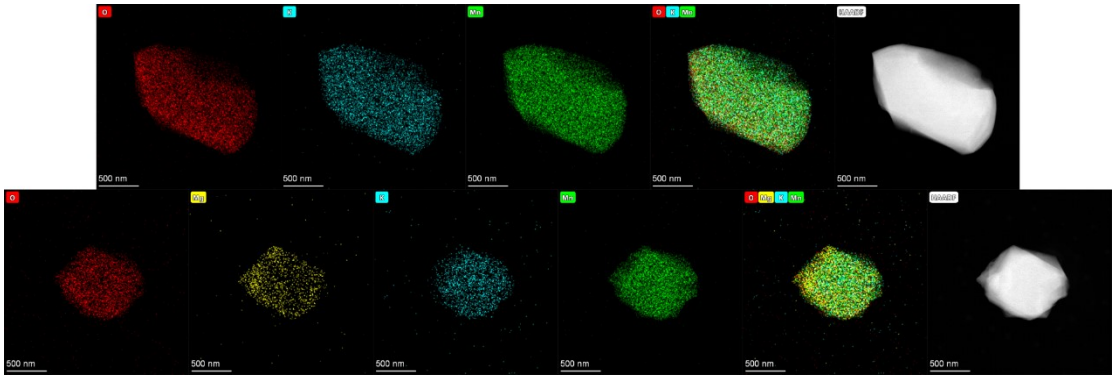

Figure S5. Element mapping of KMO and KMMO.

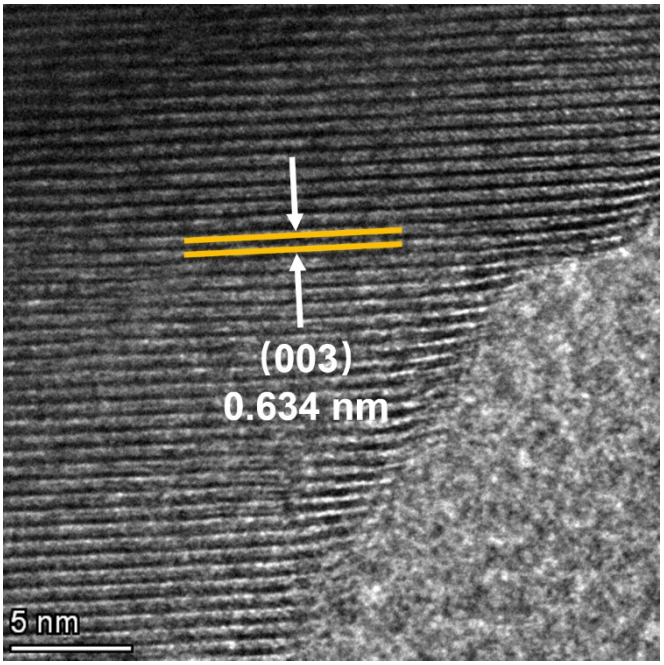

Figure S6. HRTEM images of KMO.

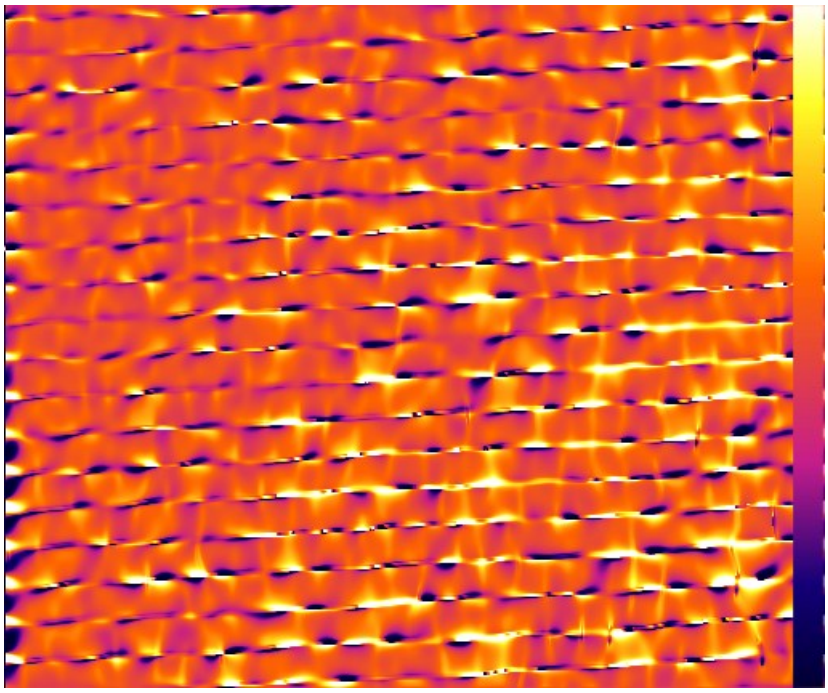

Figure S7. Strain image of KMO.

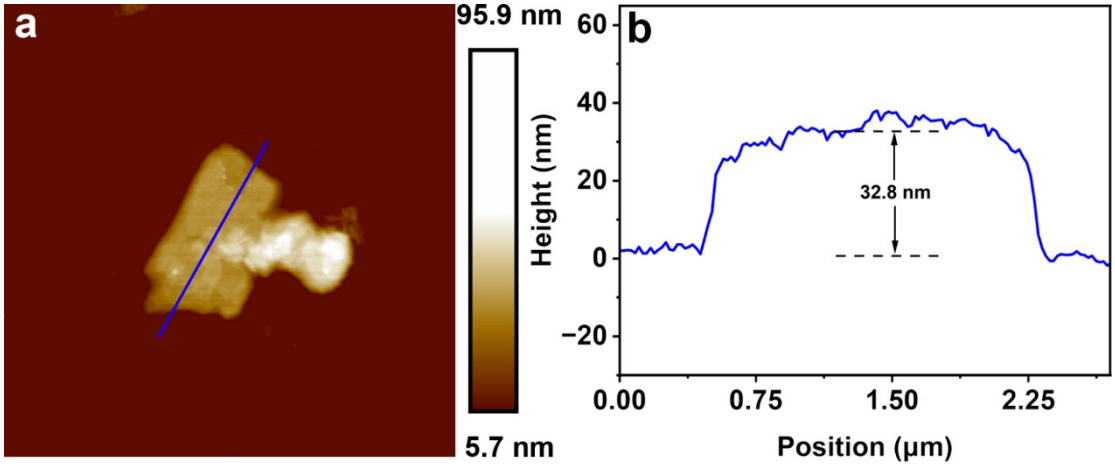

Figure S8. AFM image and corresponding profile of KMMO.

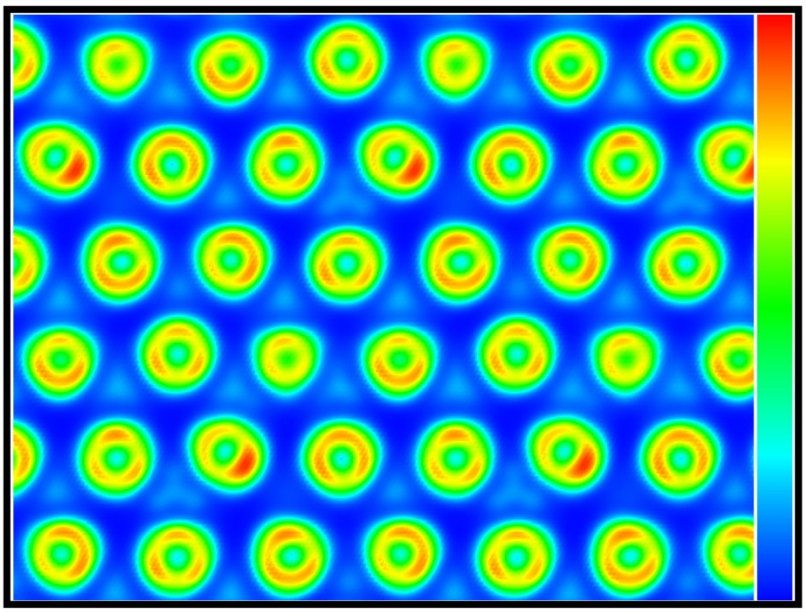

Figure S9. ELF of KMO.

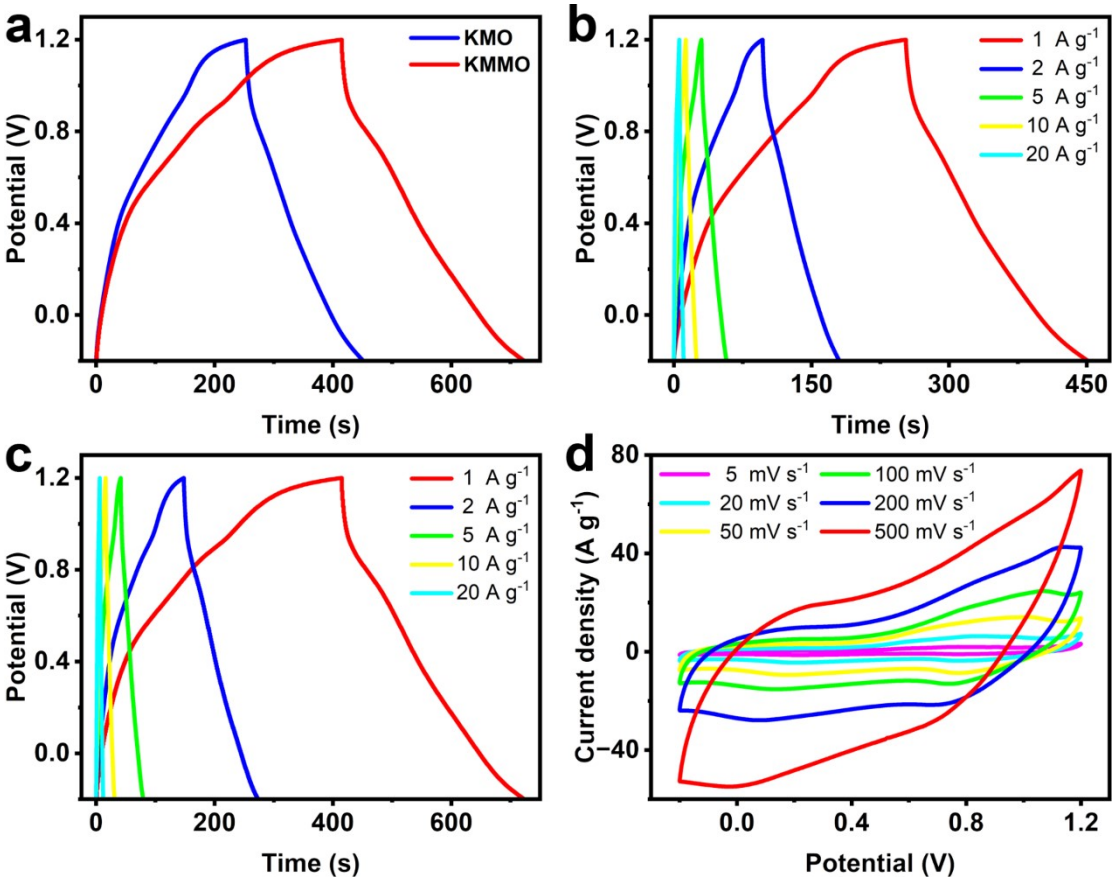

Figure S10. a) GCD curves at 1 A g^{-1} for KMO and KMMO. GCD curves at different current densities for b) KMO and c) KMMO. d) CV curves at different scan rates for KMO.

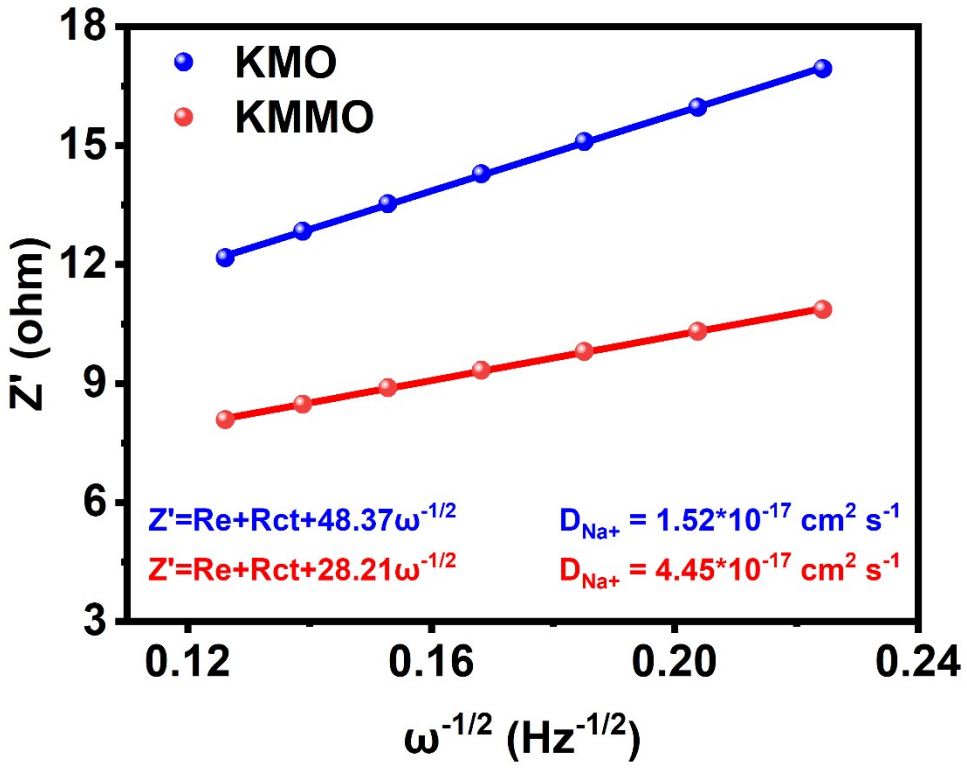

Figure S11. Low frequency Z'-$\omega^{-1/2}$ plot based on EIS measurement.

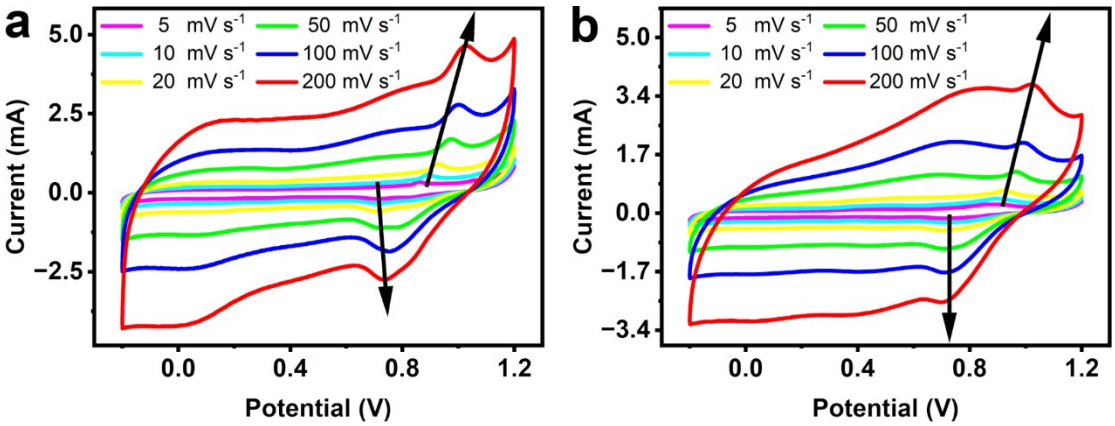

Figure S12. CV curves of a) KMO and b) KMMO at different scan rates.

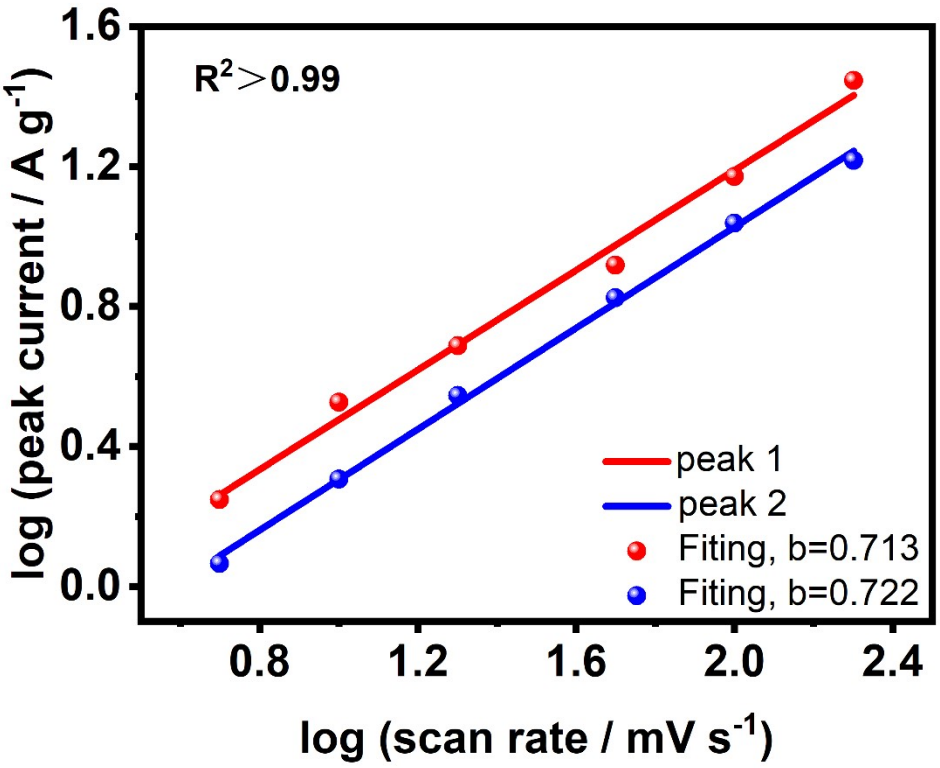

Figure S13. Relationship between peak currents and scan rates, and the corresponding b values of KMO.

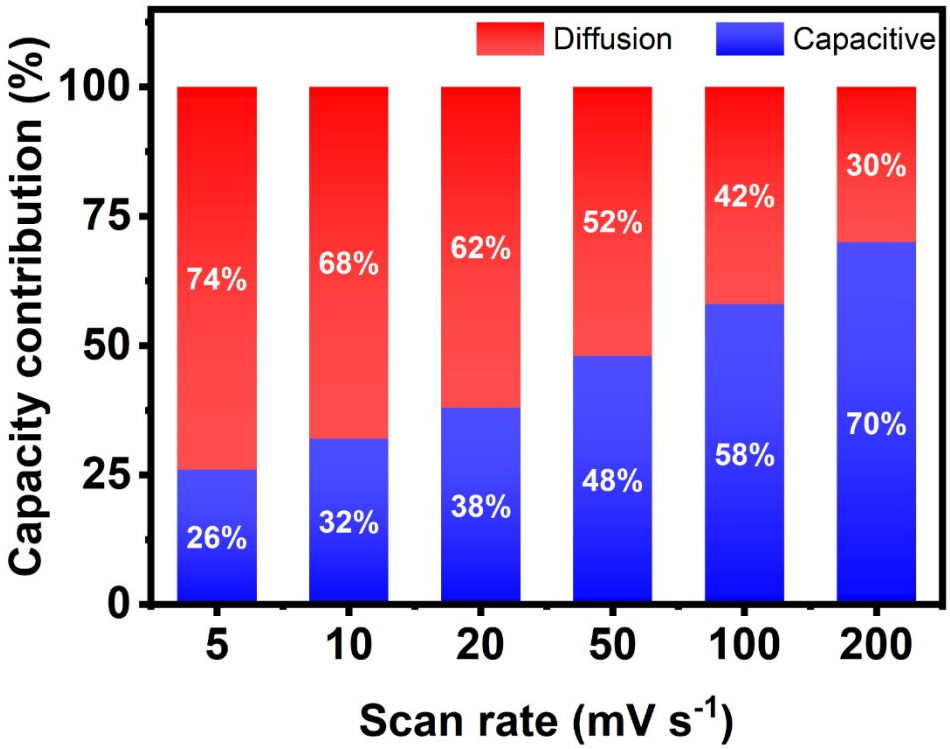

Figure S14. The contribution ratio of the capacitive and diffusion-controlled capacity versus scan rates of KMO.

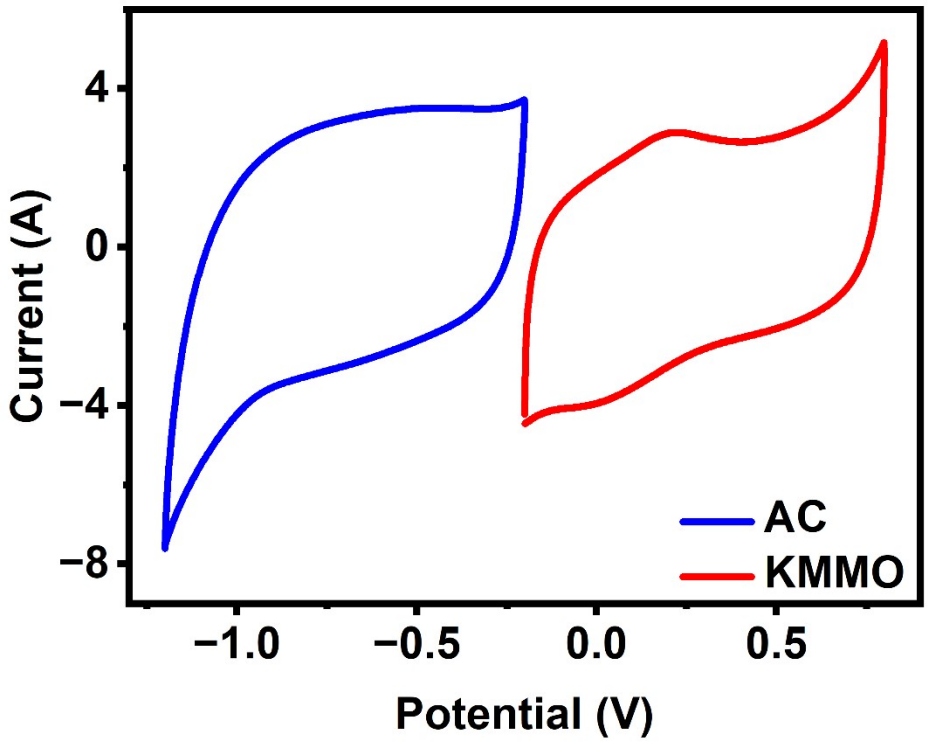

Figure S15. CV curves of KMMO and AC.

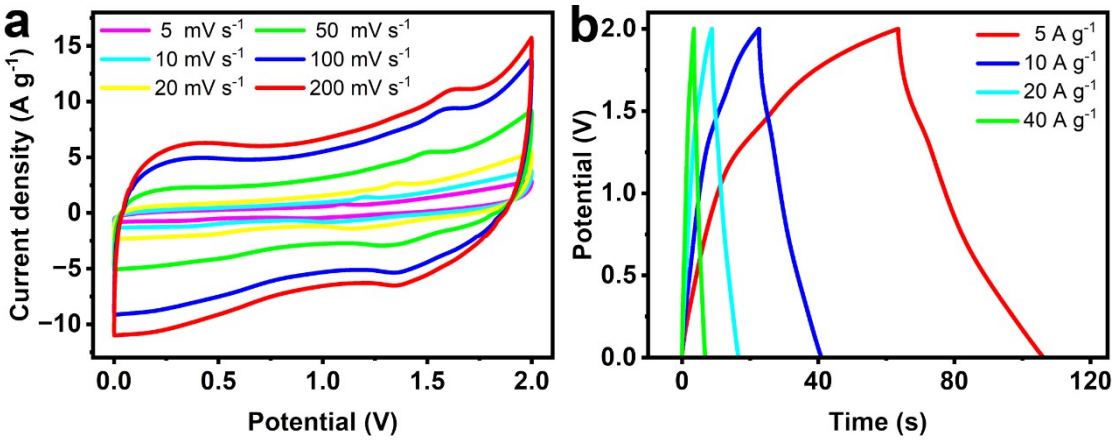

Figure S16. a) CV curves at different scan rates and b) GCD curves at different current densities of ASC.

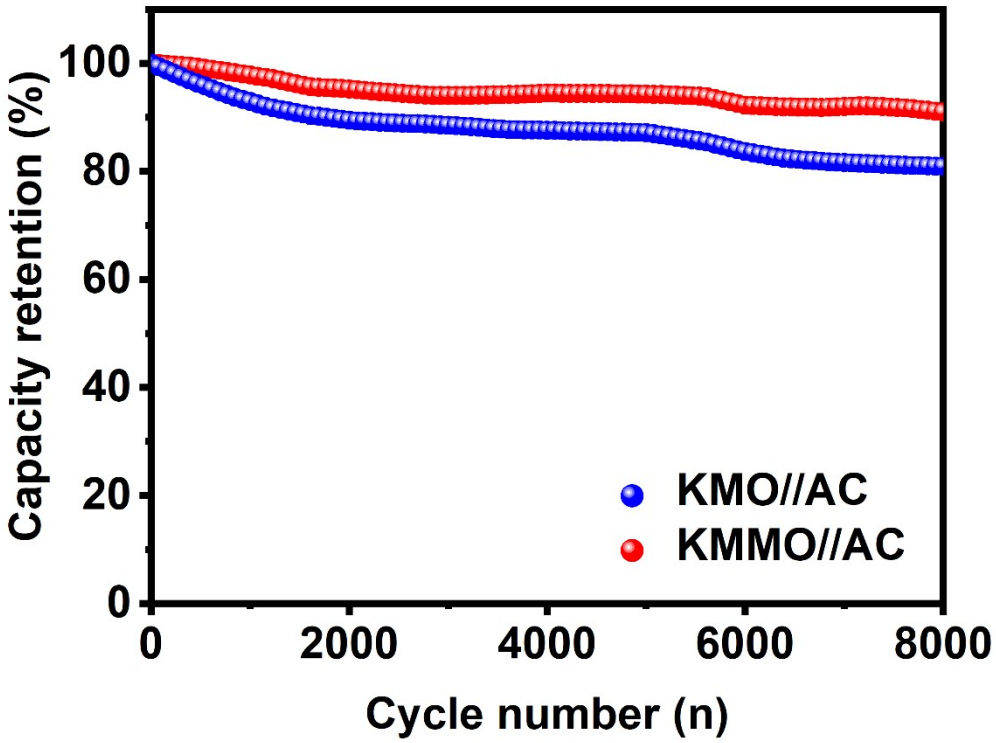

Figure S17. Cycling performance of KMO//AC and KMMO//AC at 5 A g^{-1}.

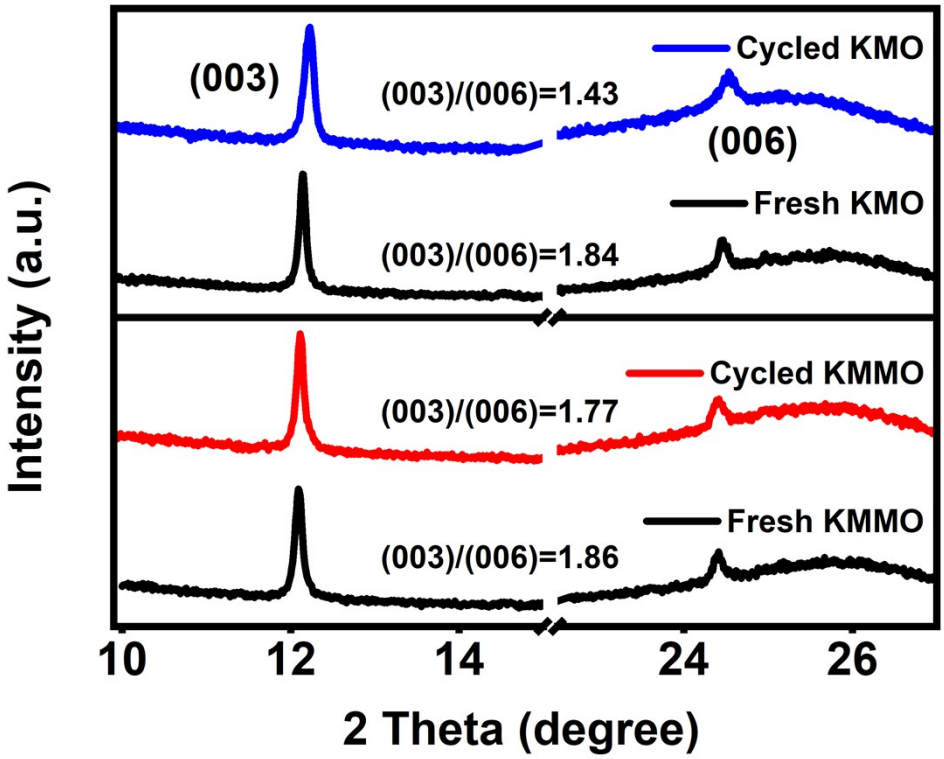

Figure S18. The XRD patterns for KMO and KMMO of fresh and after 500 cycles at 5 A g^{-1}.

Table S1. ICP-OES results for two samples.

	K	Mn	Mg
KMO	0.462	1.000	/
KMMO	0.476	1.000	0.138

Table S2. Fitting results of KMO and KMMO obtained from the EIS curves.

Sample	Rs	CPE1		Rct	W0		
		CPE1-T	CPE-P		W0-R	W0-T	W0-P
KMO	3.58	8.66×10^{-4}	0.86	8.22	58.59	0.56	0.57
KMMO	3.38	8.69×10^{-4}	0.82	4.62	71.92	0.58	0.60

References

[1] L. Y. Hu, R. Gao, A. Q. Zhang, R. Yang, X. G. Zang, S. Y. Wang, S. Y. Yao, Z. Y. Yang, H. G. Hao, Y. M. Yan, *Nano Energy* **2020**, *74*, 1044891.

[2] S. Y. Wang, R. Zhao, S. Y. Yao, B. C. Li, R. C. Liu, L. Y. Hu, A. Q. Zhang, R. Yang, X. Liu, Z. Z. Fu, D. W. Wang, Z. Y. Yang, Y. M. Yan, *J. Mater. Chem. A* **2021**, *9*, 23506-23514.

[3] A. Q. Zhang, R. Gao, L. Y. Hu, X. G. Zang, R. Yang, S. Y. Wang, S. Y. Yao, Z. Y. Yang, H. G. Hao, Y. M. Yan, *Chem. Eng. J*. **2021**, *417*, 129186.

[4] Kresse, Furthmuller, Physical review. B, Condensed matter 1996, 54, 11169-11186.

[5] G. K. A, J. F. b. J. C. M. *Science*, **1996**, *6*, 15-50.

[6] J. P. Perdew, K. Burke, M. J. P. R. L. *Phys. Rev. Lett.* **1998**, *77*, 3865-3868.